Microporous and Mesoporous Materials 368 (2024) 113008

Contents lists available at ScienceDirect

Microporous and Mesoporous Materials

journal homepage: www.elsevier.com/locate/micromeso

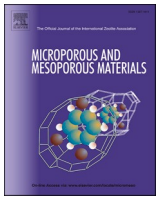

SBA-15 mesoporous particles with adsorbed cresol red dye and functionalized with 3-aminopropyl groups: Materials properties and dye release studies

Erika Švara Fabjan [a,*], Romana Cerc Korošec [b], Klara Šifrer [a,b], Andrijana Sever Škapin [a], Ramón Martínez-Máñez [c,d]

[a] Slovenian National Building and Civil Engineering Institute, Dimičeva ulica 12, 1000, Ljubljana, Slovenia
[b] University of Ljubljana, Faculty of Chemistry and Chemical Technology, Večna pot 113, 1000, Ljubljana, Slovenia
[c] Instituto Interuniversitario de Investigación de Reconocimiento Molecular y Desarrollo Tecnológico (IDM), Universitat Politècnica de Valencia, Universitat de València, Camino de Vera s/n, 46022, Valencia, Spain
[d] CIBER de Bioingeniería, Biomateriales y Nanomedicina, Instituto de Salud Carlos III, 28029, Madrid, Spain

ARTICLE INFO

Keywords:
Mesoporous materials
SBA-15
Functionalization
Tailoring the responsiveness
Sensing

ABSTRACT

Research in the field of sensing has focused on tailoring the responsiveness of materials through the variation in materials properties achieved *via* functionalization of the mesoporous matrix. pH indicator dyes capable of protonation/deprotonation reactions are known to display different forms, resulting in changes in colour. This research focused on the preparation of mesoporous substrates SBA-15 with integrated pH indicator dye *o*-cresolsulphonephtalein (cresol red) grafted with (3-aminopropy)trimethoxysilane (gaining functionalized-SBA-15 material) in order to gain a colour change response following release of the dye. UV-Vis reflectance and absorbance spectra were used to evaluate forms of cresol red. The textural properties, including specific surface area, pore size distribution and pore volume were evaluated using nitrogen sorption, and XRD analysis was conducted to evaluate crystallinity of the material and pore ordering. The presence of 3-aminopropyl groups was determined by thermal decomposition using TGA–DSC/MS. The functionalized SBA-15 materials loaded with cresol red mostly retained ordering of the pores and showed a slight reduction in surface area. Functionalization changed the surface properties of the material. In the non-functionalized SBA-15, cresol red was present in both double (H_2L) and single (HL^-) protonated forms, whereas in the functionalized SBA-15 the deprotonated L^{2-}form prevailed. Through desorption experiments cresol red was successfully desorbed from selected sample to different media. The change of colour caused by alterations in the form of the dye once released from the mesoporous silica material into the medium was confirmed. The form of cresol red released was determined by the pH of the medium.

1. Introduction

Over the last two decades, mesoporous materials, defined as materials with a pore diameter between 2 nm and 50 nm [1], have been shown to present an interesting matrix for the preparation of materials for sensing [2–4], as well as for applications related to drug delivery [5]. It is possible to control the properties of the material through their design, influencing a material's structural, morphological and textural properties, as well as *via* functionalization of the silica matrix using different functional groups. In our previous work [6], we found that water vapor adsorption can be controlled by selective hydrophobization of a mesoporous SBA-15 matrix using hydrophobic methyl silanol groups. Roghanizad et al. [7] reported on the preparation of 3-mercaptopropyltrimethoxysilne-functionalized mesoporous fibrous silica nanospheres for the adsorption of crystal violet cationic dye from aqueous media. With a focus on functionalization using amino functional groups, Szewczyk et al. [8] reported on the preparation of 3-aminopropyl-functionalized mesoporous SBA-15 and found that the total amount of cefazolin (Cef) adsorbed increased 12-fold in the modified material compared to the non-functionalized SBA-15. Balas et al. [9] reported on the preparation of MCM-41 and SBA-15 supports functionalized with amino groups and used them as matrices for the adsorption

* Corresponding author.
E-mail address: erika.svara-fabjan@zag.si (E. Švara Fabjan).

https://doi.org/10.1016/j.micromeso.2024.113008
Received 18 October 2023; Received in revised form 19 January 2024; Accepted 21 January 2024
Available online 23 January 2024

Table 1
Description of labels for the synthesized samples described within the scope of this paper.

Synthesized samples	Label used
Cresol red-as received	CR
SBA-15	MS
MS:CR[a] = 100:1	MS-CR1
MS:CR[a] = 100:3	MS-CR3
MS:CR[a] = 100:5	MS-CR5
MS:CR[a] = 100:10	MS-CR10
MS:CR[a] = 100:35	MS-CR35
SBA-15[b] functionalized with APTMS	N-MS
MS-CR1[b] functionalized with APTMS	N-MSCR1
MS-CR3[b] functionalized with APTMS	N-MS-CR3
MS-CR5[b] functionalized with APTMS	N-MS-CR5
MS-CR10[b] functionalized with APTMS	N-MS-CR10
MS-CR35[b] functionalized with APTMS	N-MS100-CR35

[a] mass ratio.
[b] 0.01 mol of APTMS per 1 g of dry sample (samples were dried for 2 h at 0.01 mbar and 90 °C).

Table 2
Preparation of the buffer solution and samples for the dye release test with the corresponding labels used: left - description of the samples; right - presentation of the labels used.

Preparation of the buffer solutions	
Description of the buffer	Label used for the buffer solution
0.1 M acetate buffer pH 3.8	a
0.1 M HEPES buffer pH 7.5	h
0.1 M glycine buffer pH 9.0	g

Preparation of the N-MS100-CR10 sample for the CR release test:			
Volume of buffer added	Dispersion (before centrifugation)	Corresponding supernatant (after centrifugation)	Corresponding precipitate (after centrifugation)
10 mL of a	a10	a10-supernatant	a10-precipitate
20 mL of a	a20	a20-supernatant	a20-precipitate
10 mL of h	h10	h10-supernatant	h10-precipitate
20 mL of h	h20	h20-supernatant	h20-precipitate
10 mL of g	g10	g10-supernatant	g10-precipitate
20 mL of g	g20	g20-supernatant	g20-precipitate

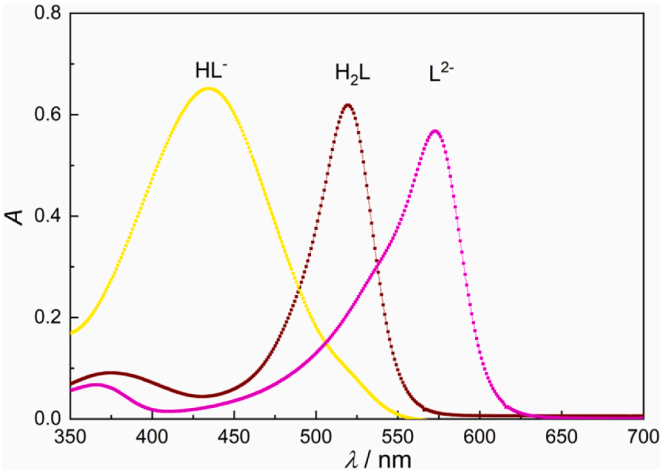

Fig. 2. UV-Vis absorbance spectra of the three forms of CR. The concentration of the doubly protonated H_2L (pH 0, purple in colour) was 0.25 mM, the singly protonated HL^-(pH 3, yellow in colour) 0.05 mM and the deprotonated L^{2-}(pH 10, violet in colour) 0.01 mM.

and release of alendronate. Wange et al. [10] prepared SBA-15 functionalized with 3-aminopropropyl for CO_2 adsorption. Very recently, Reddy et al. [11] reported on the preparation of aminosilane-modified ordered hierarchical nanostructured silica for the highly selective capture of carbon dioxide at low pressure.

Studies related to the adsorption of dyes on (meso)porous substrates are mostly aimed at the development of colorimetric/fluorometric sensors [12] or for the purpose of removing dyes from wastewater [13]. In this sphere, Huang et al. [13] described the adsorption of cationic, anionic and non-ionic dyes onto an SBA-15 matrix using fixed amounts of SBA–15 and various different dyes (cationic methylene blue (MB), anionic Reactive black 5 (RB5), neutral dimethyl phthalate (DMP) and Janus Green B (JGB)) at neutral pH. The adsorption was high for MB and JGB, but small for RB5 and DMP. It was suggested that the differences in adsorption capacities could be explained by the charge of the dyes and the zeta potential of the SBA-15 in the solution. Namely, SBA-15, which is negatively-charged, favours the adsorption of cationic species, meaning that it can be used as an effective adsorbent for removing cationic dyes from aqueous solutions. Furthermore, over recent decades

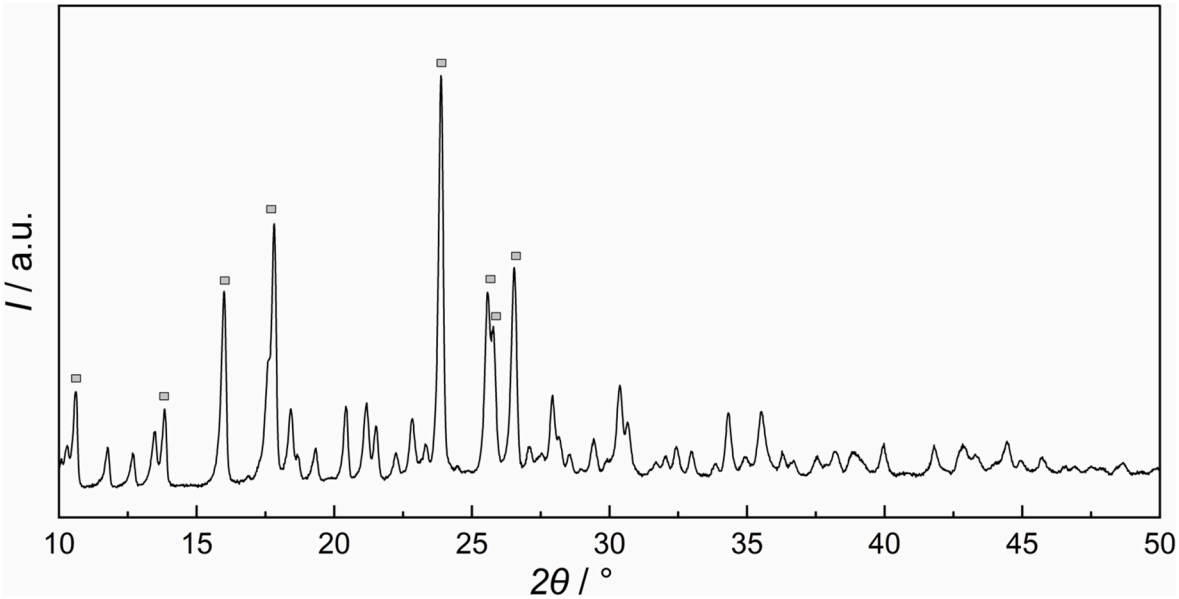

Fig. 1. XRD pattern of CR.

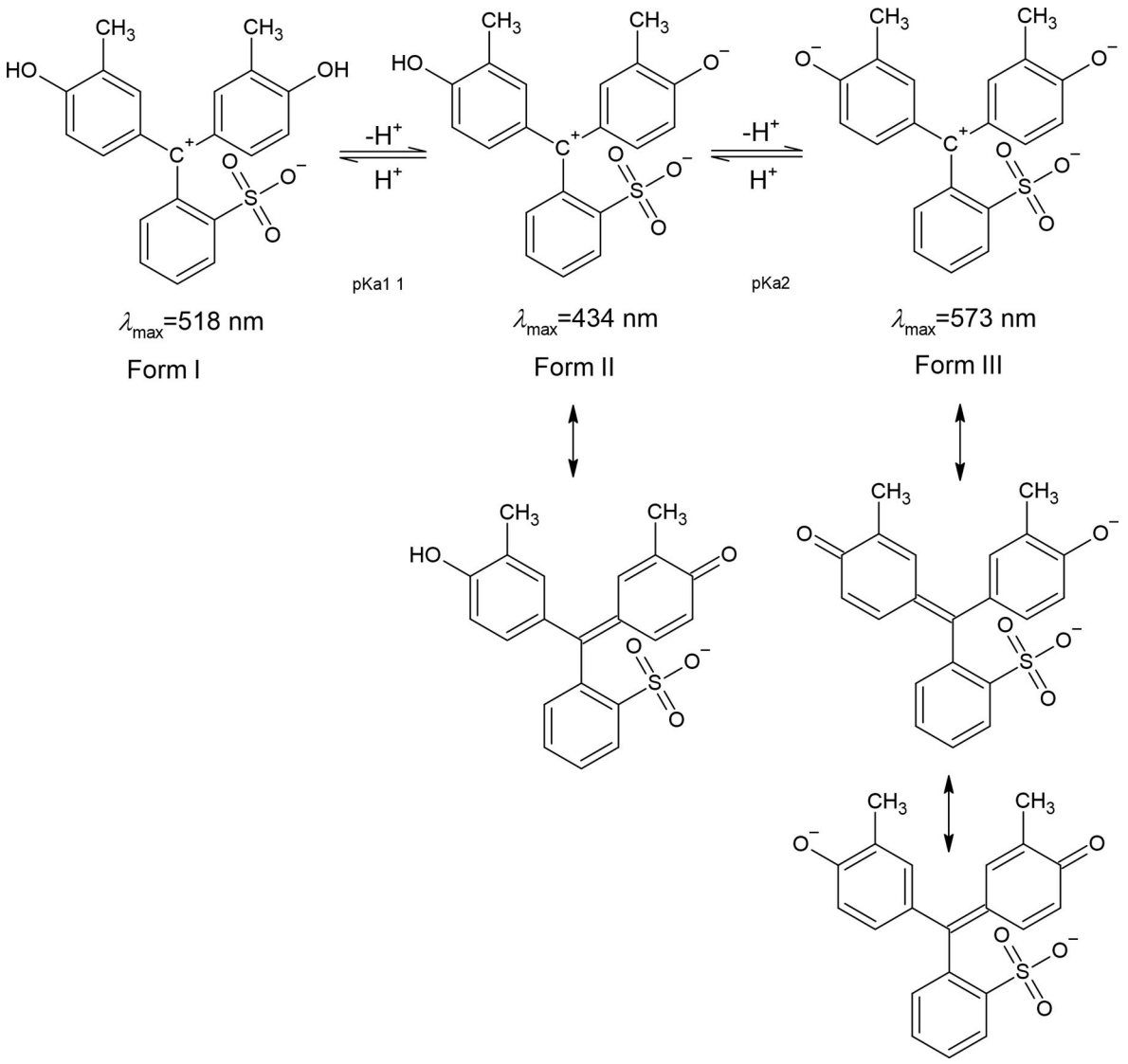

Fig. 3. Schematic representation of the aqueous forms of the CR dye. Form I ($\lambda_{max} = 518$ nm) is present in the strong acidic medium, form II ($\lambda_{max} = 434$ nm) in the mild acidic medium and form III ($\lambda_{max} = 573$ nm) in the basic medium [30].

a considerable amount of research has been published on the adsorption/desorption of chromophores/fluorophores in gated mesoporous materials for sensing applications [4,14,15]. Focusing on the adsorption and desorption of dyes in such systems, Climent et al. [12] described the loading and release of zwitterionic, neutral, anionic and cationic dyes into/from the mesoporous material MCM-41. The dyes investigated in this study were as follows: 20,70-dichlorofluorescein (F27) as the neutral dye, rhodamine 101 (Rh101) and a boron–dipyrromethene (BODIPY) derivative (BDP) as the zwitterionic dyes, rhodamine B chloride (RhB), rhodamine 101 chloride (Rh101–Cl) and rhodamine 101 perchlorate (Rh101–ClO4) as the cationic dyes, and sulforhomine B (SRB) as the anionic dye. The dyes were loaded using phosphate-buffered saline solution (PBS, pH 7.4) and acetonitrile (MeCN). The authors found that the amount of cationic rhodamines adsorbed was highest when PBS was used as the solvent, whereas the anionic and zwitterionic rhodamines were adsorbed in higher amounts when MeCN was used as the solvent [12]. Focusing on desorption of the dyes from the mesoporous matrix, the study demonstrated that the anionic dyes were released more efficiently than the cationic dyes.

Additionally, pH indicator dyes capable of protonation/deprotonation reactions are known to display different forms, depending on the selected media or substrate, resulting in changes in colour. Some studies have investigated the use of such dyes as gas sensors [16–19], but to the best to our knowledge no research exists regarding the preparation of mesoporous silica substrates with an integrated pH indicator dye in order to gain a colour change response due change of dye forms after the dye is released.

Based on the above, the aim of the present work was to prepare a mesoporous silica material loaded with a chromophore, and to study changes in the colour of the dye caused by alterations in the form of the dye once released from the mesoporous silica material into the medium. The sulphonephtalein pH indicator cresol red dye (*o*-cresolsulphonephtalein) was loaded into the SBA-15 mesoporous silica matrix and the surface of the porous support additionally functionalized using 3-aminopropyl groups. The influence of functionalization using aminopropyl groups on the spectrophotometrical, structural, textural properties of the material, as well as on the release properties of the chromophore, was studied in detail using nitrogen sorption, XRD and TGA–DSC/MS analyses, UV–Vis reflectance and absorbance spectroscopy, and the measurement of zeta potential.

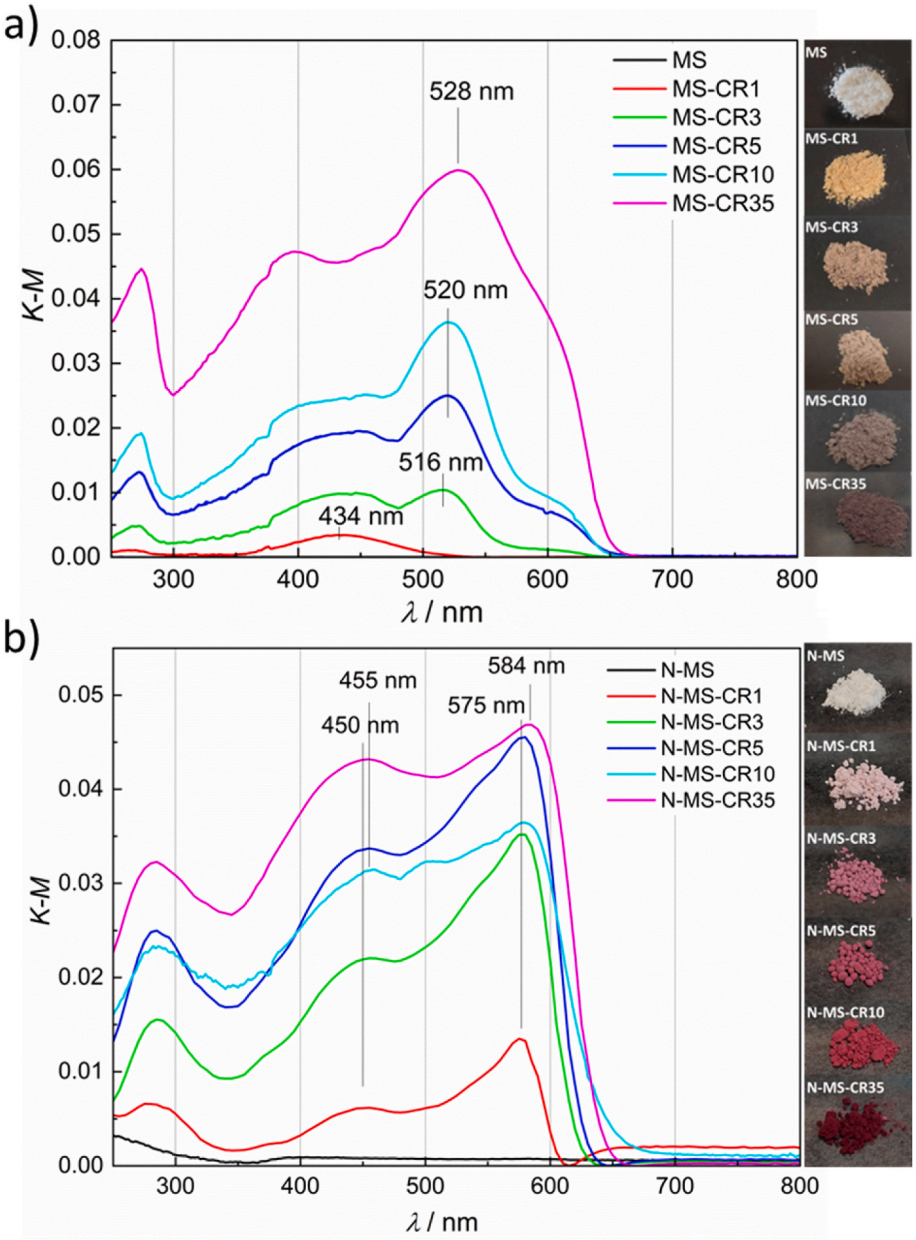

Fig. 4. Left: K-M transformations gained from the diffuse reflectance UV-Vis spectra and right: visual observation (photos) of a) the non-functionalized samples and b) the functionalized samples.

2. Materials and methods

2.1. Materials

Tetraethoxysilane (TEOS, reagent grade, 98 %), poly(ethylene glycol)–block–poly(propylene glycol)–block–poly(ethylene glycol) (Pluronic 123), acetonitrile (anhydrous 99.8 %), cresol red (CR, indicator grade, dye content 95 %), HEPES (4-(2-Hydroxyethyl)piperazine-1-ethanesulfonic acid, $C_8H_{18}N_2O_4S$, 99.5 % (titration)), sodium acetate trihydrate (ReagentPlus>99.0 %) and sodium chloride (Puriss p.a., ACS reagent, ≥99.5 %) were all purchased from Sigma–Aldrich. Hydrochloric acid (37 %) and glycine (NH_2CH_2COOH, ACS reagent, ≥98.5) were obtained from Merck S-A. Distilled water (ChromasolvTMPlus for HPLC), acetic acid (Puriss p.a., ACS reagent) and sodium hydroxide (Puriss p.a. ≥85 %) pellets were obtained from Honeywell. Barium sulphate was purchased from Fluka and 3-aminopropyltrimethoxysilane (APTMS, 97 %) obtained from abcr GmbH.

All materials were used as received.

2.2. Syntheses

2.2.1. Synthesis of the SBA-15 mesoporous material (MS)

The mesoporous Santa Barbara Amorphous 15 material (SBA–15) was synthesized using the procedures described by Zhao et al. [20] and in our previous paper [6]. Briefly, the synthesis procedure was as follows: a triblock copolymer, P123 (0.8 g) was dissolved in a mixture of HCl (37%, 20 mL) and water (96 mL), then stirred for 2 h at 35 °C. In the next step, TEOS (8.6 mL) was added drop by drop (approximately 2 drops/s). The mixture was first stirred at 35 °C for 20 h and then at 92 °C for 48 h. The molar ratio of the reagents was P123:HCl:TEOS:H_2O = 0.003:17.1:1.0:138.2. Since reports in the literature regarding the preparation of SBA-15 differ with respect to a few minor steps, further details about the synthesis are described below. Samples were synthesized in a 250 mL three necks flask connected with a condenser; the

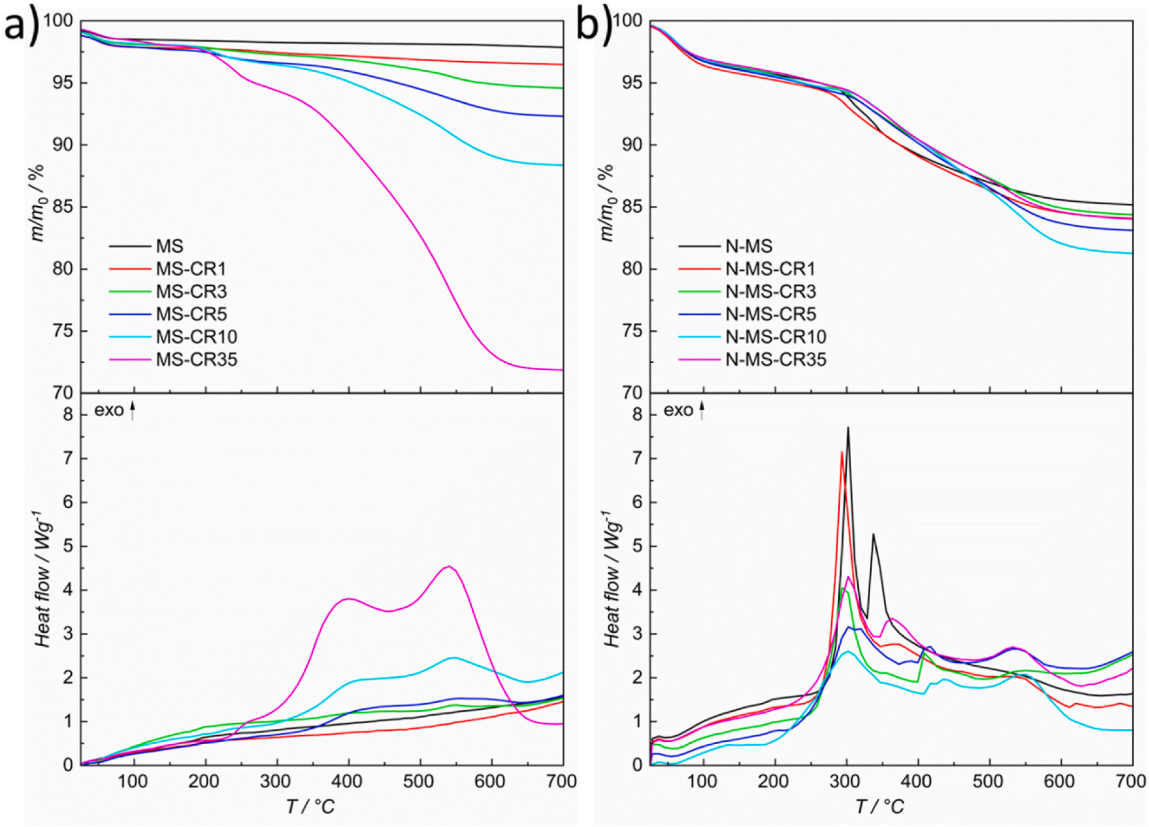

Fig. 5. TGA-DSC curves for a) non-functionalized and b) functionalized samples.

attained temperatures of 35 °C and 92 °C correspond to the temperatures measured in the reaction mixtures in the flask. The dispersion was then cooled during the stirring process and, in the next step, centrifuged for 20 min at RCF = 6080 g (8000 rpm). The precipitate was twice washed with ethanol and then dried under room conditions. The dry product was calcined in a standard air atmosphere at 550 °C using the following temperature programme: a heating rate of 1 K/min from 25 to 550 °C, followed by 360 min at 550 °C and then cooling at a rate of 2 K per minute. Finally, the samples were stored in a desiccator until required for use.

2.2.2. Loading of cresol red into SBA-15 (preparation of MS-CR)

Five different materials with CR adsorbed into MS (abbreviated to MS-CR) were prepared, varying in terms of their MS:CR weight ratio. The pre-defined mass of CR was added to the flask along with 150 mg MS and 8 mL anhydrous acetonitrile (added through the septa *via* injection) and stirred overnight for 20 h. The next day the mixture was precipitated *via* 20 min centrifugation at RCF = 6080 g (8000 rpm). The precipitated products were dried overnight under room conditions and then stored in the desiccator until required. The various mass ratios between the weighted CR and MS were as follows: MS:CR = 100:1, MS:CR = 100:3, MS:CR = 100:5, MS:CR = 100:10 and MS:CR = 100:35, their labels are presented in Table 1.

Surface functionalization of the MS and MS-CR samples with 3-aminopropyltrimethoxysilane (preparation of the N-MS and N-MS-CR samples).

Prior to functionalization with APTMS, the samples were placed in a round bottom flask and dried in a vacuum dryer at 0.01 mbar and 90 °C for 2 hurs. In order to maintain dry conditions throughout functionalization, the flask was filled with nitrogen and capped with septa and then 8 mL anhydrous acetonitrile was added. The mixture was stirred for 10 min at 300 rpm and then APTMS was added drop by drop (0.01 mol of APTMS per 1 g of the CR-loaded sample). Once the addition of APTMS was complete, the mixture was stirred overnight for 20 h under room conditions. The next day the samples were precipitated *via* centrifugation at RCF = 6080 g (8000 rpm), dried through the night under room conditions, and then stored in the desiccator until required for use. The samples were labelled according to the ratio between the amount of CR and the additional functionalization using APTMS (see Table 1).

2.3. Preparation of the samples for dye release test

2.3.1. Preparation of the buffers

0,1 mM acetate buffer with a pH of 3.8 (labelled as "a"), 0.1 M HEPES buffer with a pH of 7.5 (labelled as "h") and 0.1 M glycine buffer with a pH of 9.0 (labelled as "g") were prepared, adjusting the pH of each of the respective buffers as follows: sodium acetate with acetic acid, HEPES with 0.1 M NaOH and glycine with 0.1 M NaOH.

2.3.2. Preparation of the dispersions, the supernatants and the precipitates of the samples

The CR release test for the N-MS100-CR10 sample was performed in three different buffers (a,h,g), varying with respect to the volume added (10 mL or 20 mL). The dispersions were prepared by adding either 10 mL or 20 mL of each buffer to 5 mg of the N-MS100-CR10 sample. In the next step, the samples were stirred overnight (20 h) under room conditions. The dispersions were labelled according to the type (a, g or h) and volume (in mL i.e. 10 or 20) of the buffer added; the dispersions are therefore labelled as a10, a20, h10, h20, g10, and g20 (see Table 2). After stirring overnight, the dispersions were centrifuged at 8000 rpm. The supernatants and precipitates were then collected and analyzed *via* UV–Vis spectroscopy. For the scope of this paper the supernatants collected included a10-supernatant, a20-supernatant, h10-supernatant, h20-supernatant, g10-supernatant, g20-supernatant, while the precipitates collected included a10-precipitate, a20-precipitate, h10-precipitate, h20-precipitate, g10-precipitate and g20-precipitate.

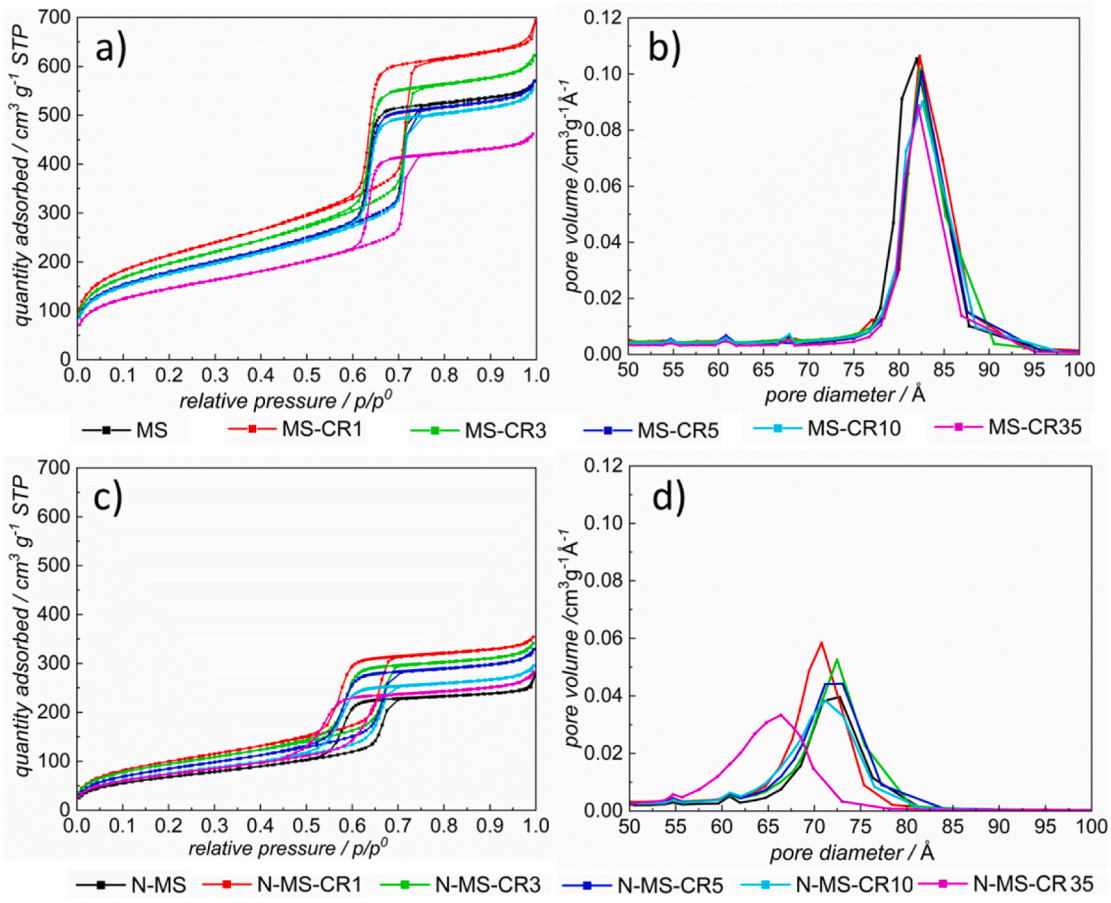

Fig. 6. a) The nitrogen sorption isotherm and b) the corresponding BJH pore size distribution for non-functionalized samples; c) the nitrogen sorption isotherm and d) the corresponding BJH pore size distribution for functionalized sampes.

The labels are presented in Table 2. The supernatants were analyzed in terms of their UV–Vis absorbance spectra, while the precipitates were analyzed using UV–Vis reflectance spectra.

2.4. Methods

2.4.1. Nitrogen physisorption

The surface area, pore size distribution and volume of pores were obtained using nitrogen physisorption. Isotherms were gained at 77 K using nitrogen sorption and an ASAP2020, Micromeritics analyzer. Approximately 80 mg of each sample was outgassed at 90 °C for 2 h and analyzed. The surface area was evaluated using the Brunauer-Emmet-Teller (BET) method [21] (abbreviated as A_{BET}), and the pore size distribution using the Barrett-Joyner-Halenda (BJH) method with the Kruk-Jaroniec-Sayari (KJS) correction from adsorption branch of isotherm [22]. The pore volume (abbreviated as *V*p) was obtained by applying the Gurvich rule at p/p^0 0.98 [21].

2.4.2. X-ray diffraction analysis (XRD)

The crystallinity and structural ordering of the pore channels of the materials were determined by X-ray diffraction (XRD), using an Empyrean diffractometer (PANalytical, The Netherlands) with Cu K_α radiation. Measurements were performed at a tube tension of 45 kV and a tube current of 40 mA, using a 2θ step size of 0.013° and a measurement time of 150 s per step. Data was collected over a 2θ range of 0.5°–80°. The results were analyzed using Highscore (PANalytical, Netherlands) diffraction software.

2.4.3. Simultaneous thermogravimetric and differential scanning calorimetry coupled with mass spectrometry (TGA–DSC/MS)

Simultaneous thermogravimetric and differential scanning calorimetry measurements (TGA–DSC) were performed using a Mettler Toledo TGA/DSC1 instrument in the temperature range between 25 °C and 700 °C. The heating rate was 10 K/min. During measurement the furnace was purged with air using a flow rate of 50 mL/min 150 μL platinum crucibles were used, while the initial mass of powdered samples was approximately 10 mg. The blank curve was subtracted for all measurements. The evolved gases were transferred to a quadrupole mass spectrometer (Pfeiffer Vacuum ThermoStar) *via* a 75-cm long heated transfer line. To lower the water content in the mass spectrometer, the sample was maintained at 25 °C for 20 min at the beginning of the measurement. Signals were collected in bar graph mode in the range from 15 to 90 *m/z*. According to expected thermal decomposition of APTMS and CR following *m/z* values were monitored: 17, 18, 30, 44, 58 and 64 *m/z*.

The calculation of mass loss of organic components was performed in the temperature range between 190 and 700 °C.

2.4.4. Zeta potential measurements

Zeta potential measurements were performed using a NanoBrook Omni Brookhaven instrument. 5 mg of each sample was dispersed in 20 mL of the buffer (abbreviated as “a”, “h”, “g”) and stirred for 30 min, then the zeta potential measurements were collected. Three measurements were performed for each sample.

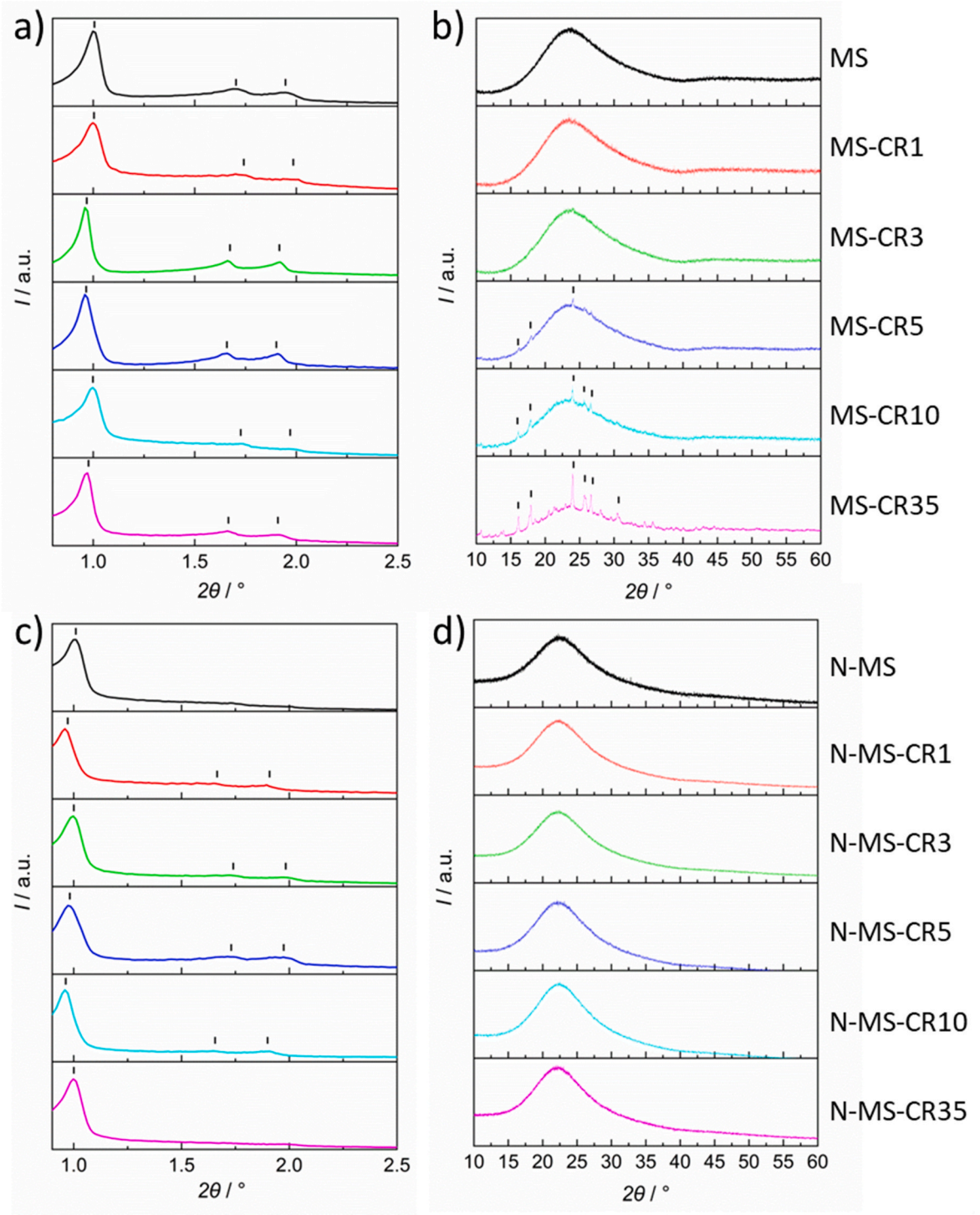

Fig. 7. Low-angle XRD patterns (a and c) and XRD patterns (b and d) for the non-functionalized and functionalized samples.

2.4.5. UV–Vis spectroscopy

2.4.5.1. UV–Vis diffuse reflectance measurements using an integrating sphere. UV–Vis diffuse reflectance of the synthesized samples was evaluated using an 150 mm integrating sphere and a Lambda 1050+ spectrophotometer (PelkinElmer). Samples were first diluted with $BaSO_4$ [23] (to form approximately 1 wt percentage mixture), using the following procedure: appropriate mass of the samples was mixed with $BaSO_4$ in an agate mortar in order to gain a homogenous mixture which was then placed in a powder sample holder (designed with a quartz cover) and data were collected. Approximately 250–300 mg of the mixture was analyzed. In order to measure diffuse reflectance (R), the specular component was excluded from the integrating sphere. Each diffuse reflectance value was then converted into the Kubelk-Munk function (K-M) or F(R) value, as described by Eq. (1). K represents the absorption, and S the scattering coefficient of the sample. Similar to the work by Davy et al. [24] and Van der Schueren et al. [25], the results are presented as reflectance spectra (Supplementary Material) and the Kubelka-Munk values.

Table 3
Specific surface area (A_{BET}), pore volumes (V_p), (d_p), lattice parameter ($d_{(100)}$), XRD unit-cell parameter (a_0) and pore wall (b_d) for the non-functionalized and functionalized samples.

Designation of samples	A_{BET}/ cm^3g^{-1}	V_p*/ cm^3g^{-1}	d_p (KJS-ads)	$d_{(100)}$/ nm	a_0/ nm	b_d/ nm
MS	651	0.85	8.2	8.7	10.1	1.9
MS-CR1	776	0.99	8.2	8.8	10.1	1.9
MS-CR3	713	0.94	8.2	9.2	10.5	2.3
MS-CR5	651	0.86	8.2	9.2	10.6	2.3
MS-CR10	637	0.82	8.3	8.8	10.1	1.9
MS-CR35	530	0.69	8.2	9.1	10.5	2.3
N-MS	255	0.38	7.3	8.7	10.0	2.7
N-MS-CR1	373	0.50	7.1	9.2	10.6	3.5
N-MS-CR3	351	0.38	7.2	8.8	10.1	2.9
N-MS-CR5	318	0.49	7.2	8.9	10.4	3.2
N-MS-CR10	282	0.44	7.1	9.2	10.6	3.5
N-MS-CR35	276	0.42	6.6	/	/	/

$$\frac{K}{S}=\frac{(1-R_\infty)^2}{2R_\infty}=F(R_\infty) \quad \text{Eq. 1}$$

2.4.5.2. UV–Vis diffuse reflectance measurements using a Praying Mantis cell and microsample holder. After the CR release test, the precipitates (see Table 2) were analyzed using a microsample holder in a Praying Mantis cell installed in a Lambda 1050+ UV/Vis spectrophotometer. Before the measurement, the specular component was decreased to below 10%. Spectralon was used as reference material. The results are presented as normalized reflectance spectra.

2.4.5.3. UV–Vis absorbance measurements. Absorbance measurements of both the supernatants and the solution were performed in microcuvettes using a Lambda 1050+ UV/Vis spectrophotometer.

In order to measure the absorbance spectra of all three forms of CR the following CR water solutions were prepared by adjusting pH using HCl and NaOH: 0.25 mM water solution (pH = 0), 0.05 mM water solution (pH = 3) and 0.01 mM water solution (pH = 10). Absorbance measurements were then performed.

3. Results and discussion

3.1. Properties of cresol red - o-cresolsulphonephtalein

Cresol red dye (*o*-cresolsulphonephtalein) belongs to the group of sulphonephtalein indicators [26], and in solid form has a quinone-like structure [27]. Similarly to phenolsulphonephtalein [28], *o*-cresolsulphonephtalein shows XRD reflections, indicating that it is crystalline. The most intensive reflections at 2θ values are seen at 10.64°, 13.85°, 16.02°, 17.85°, 23.89°, 25.57°, 26.54°, and 25.79° (the most intensive reflections are marked in Fig. 1).

In aqueous solutions, CR shows three different forms: (a) form I, doubly protonated (H_2L) in a strong acidic medium, λ_{max} at approximately 517 nm; (b) form II, singly protonated (HL^-) in a mild acidic medium, λ_{max} at approximately 432 nm; and (c) form III, deprotonated (L^{2-}) in a basic medium, λ_{max} at approximately 578 nm [29,30] (see Figs. 2 and 3)).

3.2. Properties of non-functionalized and functionalized samples with loaded CR

Fig. 4 shows the Kubelk-Munk function, KM (Experimental part, Eq. (1)), transformations obtained from the UV–Vis reflectance spectra (see the Supplementary Material for the diffuse reflectance spectra) and visual observations for the non-functionalized samples with variations in CR (Fig. 4a) and the functionalized samples using APTMS, with/without CR loaded (Fig. 4b).

As expected, the spectra of the MS sample (Fig. 4a, left) showed no bands at all in the Vis region. The sample with the smallest amount of CR (MS-CR1; Fig. 4a, left), which, according to its weight loss, contained 0.75 wt% of CR (Table S1), was yellow in colour (Fig. 4a, right) and showed a peak maximum at ca. 434 nm, suggesting that the CR is in the singly protonated form (Figs. 2 and 3). The samples with a higher amount of adsorbed CR, namely MS-CR3, MS-CR5, and MS-CR10, were brown to violet in colour (see Fig. 4a, right), and contained 2.8 wt%, 4.7 wt% and 8.9 wt% CR, respectively (Table S1). These samples showed two maximum peaks in the Vis region: at approximately 430–450 nm (broad peak) and 520 nm (Fig. 4a, left). These results are in agreement with Nahhal et al. [31], who immobilized CR into a silica network using a sol-gel process, and also observed two absorption bands, at 449 nm and 525 nm, they observed the red shift of the 435 nm peak ca 14 nm for immobilized CR into silica [31]. According to the different forms of the CR (Figs. 2 and 3), it is suggested that both, singly and doubly protonated forms of CR were present in the sample, whereby partial protonation was attributed to silanol groups [31]. In the work of Nahhal et al. [31] the existence of the doubly-protonated form of CR was suggested, what they explain indicated the influence of an added supplement, which could acted as a source for protonation and results in strong electrostatic interaction between compounds [31]. Since, in our research work, MS without any other additives was used for the loading of CR, this could be the influence of the CR concentration, or the way in which CR was loaded with different concentrations in the MS material. In the next step, the effect of the functionalization of the surfaces of the MS and MS-CR samples using 3-aminopropyl groups (APTMS) was studied. The spectra of the APTMS-functionalized MS samples loaded with CR are shown in Fig. 4b; all of them are violet in colour (Fig. 4b, right), with the darker colour indicating that a higher percentage of CR was loaded. All spectra showed two peaks in the Vis region, one between $\lambda = 450$ and $\lambda = 455$ nm and more intense peak maximum between $\lambda = 575$ and $\lambda = 585$ nm. It is proposed that the peak maximum at 576 nm is due to the partial ionization of CR and the equilibrium shifting to the right [30] (see Fig. 3), L^{2-} form. Since the surface of the N-MS-CR samples was functionalized using basic amino groups, we propose that CR was obtained in its deprotonated form in all the samples, confirming the more basic properties of the N-MS matrix. The peak maximum at approximately $\lambda = 450$ nm corresponds to the HL^- form. We therefore suggested the presence of L^{2-} and HL^- forms in the functionalized samples.

The TGA-DSC curves of the samples with adsorbed CR and additionally functionalized are presented in Fig. 5a and b, respectively. In the samples with loaded CR, the mass loss over the entire temperature range (25–700°) gradually increases from MS-CR1 to MS-CR35. The mass loss (used for the evaluation of CR loss) of the samples determined in temperature range between 190 and 700 °C was between 0.54 and 25,87% (Table S1). In samples with a higher CR load the DSC curves exhibit two exothermic peaks, positioned at approximately 400 °C and 550 °C (Fig. 5a - left). In the functionalized samples the mass loss is quite similar for the samples with a different CR load, ranging from 14% to 18% (Fig. 5b). The largest mass loss is observed in the sample N-MS-CR10, while in the non-functionalized samples the sample MS-CR35 exhibited the highest mass loss. We propose there was a dye elution during the process of functionalization, which resulted in reduced amount of loaded CR in functionalized materials.

The thermal degradation of functionalized samples is in agreement with the literature report showing continuous decrease in mass with temperature due degradation and evaporation of 3-aminopropyl grafted molecules [8]. Since the thermal degradation of CR occurs in a similar temperature range (Fig. 5), we could not separate the thermal degradation of the CR and aminopropyl groups in the sample. The additional sharp exothermic peak at around 300 °C (Fig. 5b), most probably reflects the thermal decomposition of APTMS.

In order to confirm the aminopropyl groups in the functionalized sample a comparison of coupled TGAMS measurements of the CR, MS-

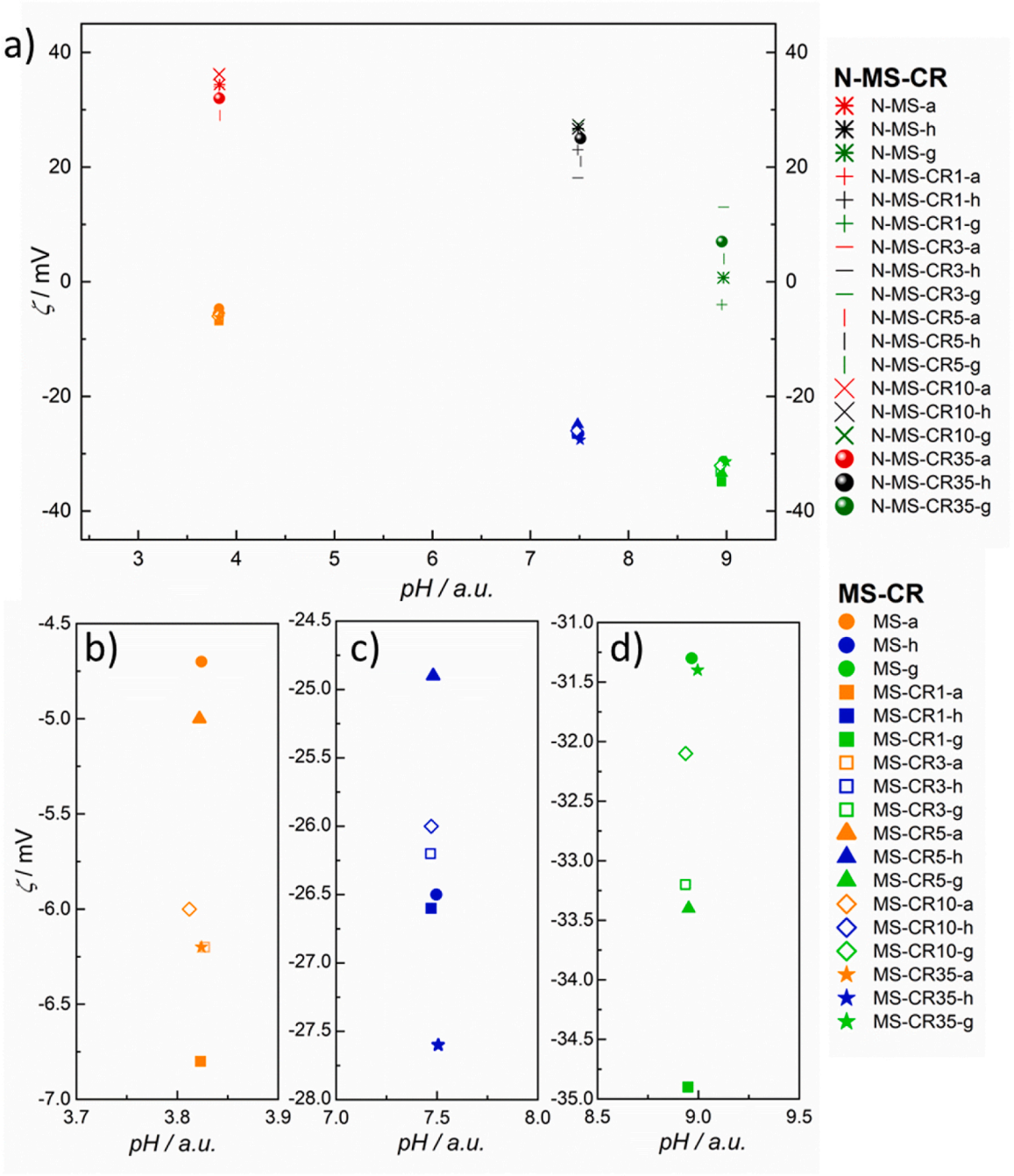

Fig. 8. a) Zeta potential of the non-functionalized (MS-CR; shown in orange, blue and light green) and functionalized samples (N-MS-CR, shown in red, black and dark green), measured at pH values of 3.8, 7.5 and 9.0. The insets of zeta potentials for MS-CR samples: b) for the samples measured in the "a" buffer, c) for the samples measured in the "h" buffer, and d) for samples measured in the "g" buffer.

CR10 and N-MS-CR10 was carried out (Fig. S2). The thermal decomposition of CR and MS-CR10 resulted in signals at 17, 18, 44, and 64 *m/z* (Fig. S2a and Fig. S2b). The first two signals are typical for water evolution, whilst the signal at 64 *m/z* corresponds to SO_2. Since cresol red contains a sulphur atom, the evolution of SO_2 is a clear indication of its decomposition. It is suggested that signals at 44 *m/z* correspond to CO_2 due thermal decomposition of organic components. Since the signal is also present in the non-functionalized samples, it could not be used for further evaluation of the fragment $H_2N–CH_2–CH_2^+$ at 44 *m/z* as reported by Zarinwall et al. [32]. The TGA-MS curves of the functionalized sample N-MS-CR10 (Fig. S2c) confirm the presence of the same signals as for non-functionalized one namely at 17, 18, 44, 64 *m/z* and additional signals at 30 and 58 *m/z*. We propose the additional signal at 58 *m/z* corresponds to the fragment of thermal degradation of the aminopropyl moiety [32,33]. Qiao et al. described that in this process group $NH_2CH_2CH_2CH_2$. is released [34]. Consequently we propose that signal at 58 *m/z* belongs to fragment $H_2N–CH_2–CH_2–CH_2^+$. The signal at 30 *m/z* could corresponds to the fragment confirming the presence of NO_2 [35] as result of thermal decomposition of amino groups.

The nitrogen sorption isotherms and pore size distribution of the non-functionalized samples, with and without CR loaded are shown in Fig. 6a and b, respectively, while the results of the functionalized samples are shown in Fig. 6c and d. The isotherms of all samples (Fig. 6a and c) correspond to the type IV isotherm typical of mesoporous materials, in

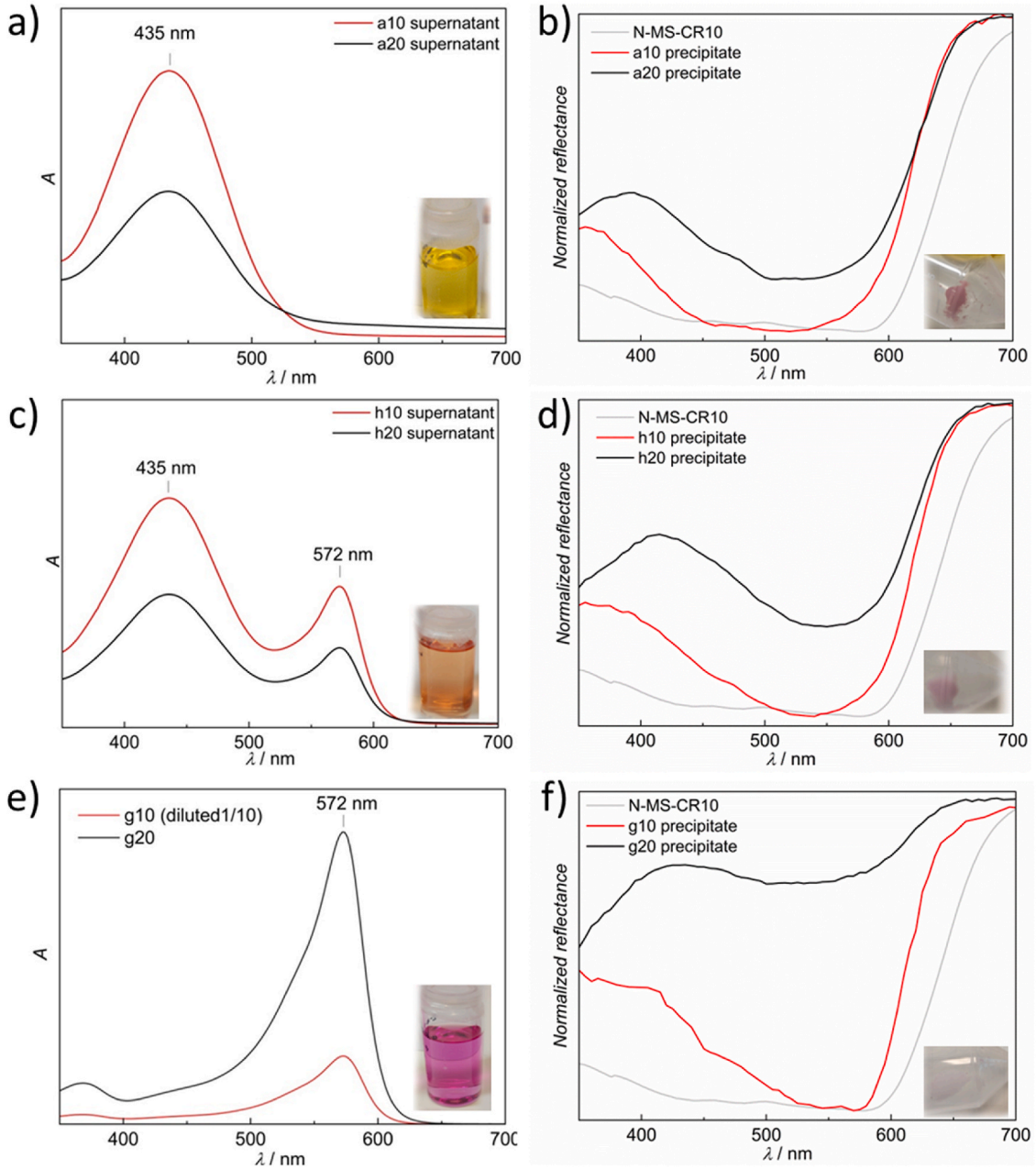

Fig. 9. CR release test for the functionalized sample, N-MS-CR10: The UV–Vis absorbance spectra of supernatants (9.a, 9.c and 9.e) and UV–Vis reflectance spectra of precipitates (9.b, 9.d and 9.f).

which the initial monolayer-multilayer adsorption of N_2 is followed by condensation in the pores. Lower amounts of the adsorbed CR resulted in materials with slightly increased specific surface area, suggesting different sorption processes of very diluted solutions of CR, which could resulted in partial sorption of CR to outer surface area of MS. With higher amounts of CR (MS-CR10 and MS-CR35), the surface area and volume of pores are reduced, suggesting the CR was loaded into the pore channels.

Moreover, the quantity of adsorbed nitrogen was lower after functionalization (Fig. 6c in comparison to Fig. 6a), suggesting binding of aminopropyl groups to the MS surface. The lowest quantities were adsorbed in the sample without CR (black curve) and the sample with the highest amount of CR (pink curve), these samples also exhibiting the lowest surface area. We assumed the CR load to pore channels and aminopropyl groups bind to the MS. The volume of pores decreased when a higher amount of CR was adsorbed, suggesting due CR loading to pore channels at higher amounts and aminopropyl groups were partially bound also to internal surface of pore channels, but did not close the pore channels.

X-ray diffraction was used to analyze the ordering of the pores (Fig. 7a) and the crystallinity of the materials (Fig. 7b). All non-functionalized material exhibited three peaks in low-angle diffraction patterns (see Fig. 7a), which is in agreement with the pattern of the mesoporous SBA-15 material [22]. The peaks can be indexed on a hexagonal lattice for the p6mm hexagonal symmetry as (100), (110) and (200) reflections. The lattice parameter at (100) reflection ($d_{(100)}$) and the calculated XRD unit-cell parameter (a_0) and pore wall (b_d) are shown in Table 3. The XRD unit-cell parameter of the non-functionalized samples with variation in CR ratio and calculated pore wall did not change significantly after CR loading. The XRD patterns for the

non-functionalized mesoporous materials are presented in Fig. 7b. The MS material (the upper black curve) confirms the presence of amorphous material (by the presence of a broad peak) and the absence of crystallinity. The same behaviour was found in the materials MS-CR1 and MS-CR3. The materials MS-CR5, MS-CR10 and MS-CR35 showed additional peaks at ca. 16.1°, 17.9°, 24.0°, 25.8° and 26.6° 2θ, which correspond to the presence of the crystalline CR phase in the sample.

The low-angle diffraction patterns of the functionalized samples N-MS-CR1, N-MS-CR3, N-MS-CR5 and N-MS-CR10, exhibit three peaks (see Fig. 7c – red, green, blue and cyan patterns) characteristic of hexagonally ordered structure which are also observed upon functionalization with APTMS and CR loading. But for the samples N-MS and N-MS-CR35 (110) and (200) reflections are not visible in their low angle XRD patterns (Fig. 7c – black and magenta patterns). The XRD unit-cell parameter of the functionalized samples with loaded CR did not change significantly, but due reducing the pore diameter of those samples the pore wall suggested to increase (b_d, Table 3). XRD analysis confirms the presence of a broad peak between 15° and 25° 2θ in all functionalized samples (Fig. 7b and c), corresponding to amorphous SiO_2. Moreover, no additional peaks were observed between 20° and 80° 2θ, suggesting that CR is not in crystalline form in deprotonated form L^{2-} present in the amine-functionalized materials (confirmed using UV–Vis spectra, Fig. 4)

Zeta potential measurements were performed to evaluate the influence of surface functionalization using APTMS on the colloidal stability and charge of the non-functionalized and functionalized samples in three different buffers ("a", "h" and "g"). The results are shown in Fig. 8. The zeta potentials for the non-functionalized samples show similar behaviour both with and without CR. Zeta potentials for the non-functionalized samples are between −5 mV and −7 mV in the "a" buffer (Fig. 8b), −25 mV and −28 mV in the "h" buffer (Fig. 8c); and −31 mV and −35 mV in the "g" buffer (Fig. 8d). It can be concluded that the presence of CR did not affect the zeta potential compared with the unloaded sample. The amino-functionalized samples containing CR, however, show similar behaviour to the N-MS sample (Fig. 8), with the zeta potentials for samples between 29 mV and 36 mV in the "a" buffer, 18 mV and 27 mV in the "h" buffer, and 13 mV and −5 mV in the "g" buffer. As expected, the nitrogen-functionalized samples displayed more positive values than the unfunctionalized solids. The approximate point of zero zeta potential for the non-functionalized samples was observed to be at an acidic pH (pH 3 and pH 4), whereas it was around pH = 9 in the functionalized samples.

The CR dye release tests were performed on the functionalized sample N-MS-CR10. The supernatants and precipitates were collected and analyzed (see Fig. 9a). Before the CR release test the functionalized sample N-MS-CR10 was violet in colour, with peak maximum at approximately 574 nm suggesting the presence of CR in deprotonated form L^{2-} (Fig. 4). The CR released from the sample N-MS-CR10 in the "a" buffer (a10 supernatant and a20 supernatant) are yellow in colour, with the presence of an absorbance peak at 435 nm (Fig. 9a), confirming the presence of CR in form II (singly protonated HL^-) after release to buffer "a". The CR remaining in the sample N-MS-CR10 after the CR release test (a10 precipitate and a20 precipitate) remain violet in colour (see the spectra and photo of a10 precipitate in Fig. 9b), and the UV-Vis reflectance spectra show decreased reflectance between 460 and 550 nm. The CR released from the sample N-MS-CR10 in the "h" buffer (h10 supernatant and h20 supernatant) are orange in colour and the UV–Vis absorbance spectra of the supernatants show the presence of absorption bands at 435 nm and 572 nm, confirming the presence of singly protonated HL^- and deprotonated L^{2-} forms of CR (Fig. 9c). The CR remaining in the sample N-MS-CR10 after the CR release test (h10 precipitate and h20 precipitate) remains violet in colour (Fig. 9d), with a decrease in the reflectance spectra in the region between 500 and 600 nm. In the "g" buffer, the CR released from this sample (g10 supernatant and g20 supernatant) were violet in colour and the UV–Vis absorbance spectra show the presence of absorbance peaks at 572 nm in both samples (see the photo and spectra in Fig. 9e), confirming the presence of CR in form III (deprotonated L^{2-} form, see Fig. 4). In this case, any CR remains in the sample (h10 precipitate and h20 precipitate) following completion of the CR release test was light violet in colour (Fig. 9f), and the reflectance spectra show that reflectance decreased most between 500 and 600 nm.

It is clear from these experiments that the CR was successfully desorbed from the sample N-MS-CR10 to the different media. The form of CR released was influenced by the pH of the medium (the presence of singly protonated HL^- form in buffer "a", the presence of singly protonated HL and deprotonated L^{2-} forms in buffer "h", and the presence of deprotonated form L^{2-} in buffer "g"). Given that the reflectance decreased most between 500 and 600 nm, and the remained violet colour of all the materials after release test, it is suggested that CR remaining in the sample N-MS-CR10 gains mostly in the deprotonated form L^{2-}, the same as before CR release test.

4. Conclusion

In this study we successfully prepared of SBA-15 material with adsorbed cresol red dye and functionalized the surface using 3-aminopropyl groups. Non-functionalized samples with various cresol red weight ratios retained their porous structure. The zeta potential of all samples was similar to the non-functionalized SBA-15 material. Following 3-aminopropyl functionalization the porous structure SBA-15 materials loaded with *o*-cresolsulphonephtalein mostly showed a slightly reduced surface area, whilst the ordering of the pores was mostly retained. Functionalization changes the surface properties of the mesoporous silica and influences the chemical reaction with the loaded cresol red. In the non-functionalized SBA-15 cresol red is present in both double (H_2L) and singly (HL^-) protonated forms. Moreover, in the non-functionalized samples we discovered the influence of cresol red concentration samples on its resulting form: a lower concentration results in the single protonated form, while in the higher concentrated samples it is present in its double protonated form. On the contrary, in the 3-aminopropyl functionalized SBA-15 is mostly present in the deprotonated L^{2-} form. Through cresol red desorption experiments it has been proved cresol red was successfully desorbed from the selected sample to the different media. The form of cresol red released was determined by the pH of the medium (the presence of singly-protonated HL at a buffer pH of 3.8, the presence of singly protonated HL^- and deprotonated L^{2-} at a buffer pH of 7.5, and the presence of the deprotonated form L^{2-} at a buffer pH of 9). It is suggested that any CR remaining in the sample following the release test was mostly present in the deprotonated form, L^{2-}, the same form as was present prior to the CR release test. The mechanism of changes in the colour of the dye caused by alterations in the form of the dye once released from the mesoporous silica material into the medium, present potential in sensing applications in combination with gated materials and further work in this area will be carried out in due course.

CRediT authorship contribution statement

Erika Švara Fabjan: Writing – review & editing, Writing – original draft, Supervision, Investigation, Conceptualization. **Romana Cerc Korošec:** Writing – review & editing, Writing – original draft, Investigation. **Klara Šifrer:** Investigation. **Andrijana Sever Škapin:** Writing – review & editing, Funding acquisition. **Ramón Martínez-Máñez:** Writing – review & editing, Conceptualization.

Declaration of competing interest

The authors declare that they have no known competing financial interests or personal relationships that could have appeared to influence the work reported in this paper.

Data availability

Data will be made available on request.

Acknowledgments

We acknowledge the financial support from the Slovenian Research and Innovation Agency through core research Programmes No. P2–0273 and No. P1–0134. This research was also supported by projects PID2021-126304OB-C41 and PID2021-128141OB-C22 funded by MCIN/AEI/10.13039/501100011033/ and by European Regional Development Fund - A way of doing Europe. This study was also supported by Generalitat Valenciana (CIPROM/2021/007). We are very grateful to Catherine Earles for proofreading the English manuscript.

Appendix A. Supplementary data

Supplementary data to this article can be found online at https://doi.org/10.1016/j.micromeso.2024.113008.

References

[1] J. Rouquerol, D. Avnir, C.W. Fairbridge, D.H. Everett, J.M. Haynes, N. Pernicone, J. D.F. Ramsay, K.S.W. Sing, K.K. Unger, Recommendations for the characterization of porous solids (technical report), Pure Appl. Chem. 66 (8) (1994) 1739–1758, https://doi.org/10.1351/pac199466081739.

[2] M. Gao, J. Zeng, K. Liang, D. Zhao, B. Kong, Interfacial assembly of mesoporous silica-based optical heterostructures for sensing applications, Adv. Funct. Mater. 30 (9) (2020) 1906950, https://doi.org/10.1002/adfm.201906950.

[3] F. Luo, C. Long, Z. Wu, H. Xiong, M. Chen, X. Zhang, W. Wen, S. Wang, Functional silica nanospheres for sensitive detection of H9N2 avian influenza virus based on immunomagnetic separation, Sensor. Actuator. B Chem. 310 (2020) 127831, https://doi.org/10.1016/j.snb.2020.127831.

[4] E. Climent, M. Biyikal, D. Gröninger, M.G. Weller, R. Martínez-Máñez, K. Rurack, Multiplexed detection of analytes on single test strips with antibody-gated indicator-releasing mesoporous nanoparticles, Angew. Chem. Int. Ed. 59 (52) (2020) 23862–23869, https://doi.org/10.1002/anie.202009000.

[5] M. Vallet-Regí, F. Schüth, D. Lozano, M. Colilla, M. Manzano, Engineering mesoporous silica nanoparticles for drug delivery: where are we after two decades? Chem. Soc. Rev. 51 (13) (2022) 5365–5451, https://doi.org/10.1039/D1CS00659B.

[6] E. Švara Fabjan, P. Nadrah, A. Ajdovec, M. Tomšič, G. Dražić, M. Mazaj, N. Zabukovec Logar, A. Sever Škapin, Colorimetric cutoff indication of relative humidity based on selectively functionalized mesoporous silica, Sensor. Actuator. B Chem. 316 (2020) 128138, https://doi.org/10.1016/j.snb.2020.128138.

[7] A. Roghanizad, M. Karimi Abdolmaleki, S.M. Ghoreishi, M. Dinari, One-pot synthesis of functionalized mesoporous fibrous silica nanospheres for dye adsorption: isotherm, kinetic, and thermodynamic studies, J. Mol. Liq. 300 (2020) 112367, https://doi.org/10.1016/j.molliq.2019.112367.

[8] A. Szewczyk, M. Prokopowicz, W. Sawicki, D. Majda, G. Walker, Aminopropyl-functionalized mesoporous silica SBA-15 as drug carrier for cefazolin: adsorption profiles, release studies, and mineralization potential, Microporous Mesoporous Mater. 274 (2019) 113–126, https://doi.org/10.1016/j.micromeso.2018.07.046.

[9] F. Balas, M. Manzano, P. Horcajada, M. Vallet-Regí, Confinement and controlled release of bisphosphonates on ordered mesoporous silica-based materials, J. Am. Chem. Soc. 128 (25) (2006) 8116–8117, https://doi.org/10.1021/ja062286z.

[10] L. Wang, R.T. Yang, Increasing selective CO2 adsorption on amine-grafted SBA-15 by increasing silanol density, J. Phys. Chem. C 115 (43) (2011) 21264–21272, https://doi.org/10.1021/jp206976d.

[11] K.S.K. Reddy, A.M. Varghese, A.E. Ogungbenro, G.N. Karanikolos, Aminosilane-modified ordered hierarchical nanostructured silica for highly-selective carbon dioxide capture at low pressure, ACS Applied Engineering Materials 1 (2) (2023) 720–733, https://doi.org/10.1021/acsaenm.2c00136.

[12] E. Climent, M. Hecht, K. Rurack, Loading and release of charged and neutral fluorescent dyes into and from mesoporous materials: a key role for sensing applications, Micromachines 12 (3) (2021) 249, https://doi.org/10.3390/mi12030249.

[13] C.-H. Huang, K.-P. Chang, H.-D. Ou, Y.-C. Chiang, C.-F. Wang, Adsorption of cationic dyes onto mesoporous silica, Microporous Mesoporous Mater. 141 (1–3) (2011) 102–109, https://doi.org/10.1016/j.micromeso.2010.11.002.

[14] F. Sancenón, L. Pascual, M. Oroval, E. Aznar, R. Martínez-Máñez, Gated silica mesoporous materials in sensing applications, ChemistryOpen 4 (4) (2015) 418–437, https://doi.org/10.1002/open.201500053.

[15] Hernández-Montoto, A.; Aranda, M. N.; Caballos, I.; López-Palacios, A.; Tormo-Mas, M. Á.; Pemán, J.; Rodríguez, M. P.; Picornell, C.; Aznar, E.; Martínez-Máñez, R. Human Papilloma Virus DNA Detection in Clinical Samples Using Fluorogenic Probes Based on Oligonucleotide Gated Nanoporous Anodic Alumina Films. Advanced Healthcare Materials n/a (n/a), 2203326. https://doi.org/10.1002/adhm.202203326..

[16] S. Islam, N. Bidin, S. Riaz, R.A. Rahman, S. Naseem, F.M. Marsin, Mesoporous SiO2–TiO2 nanocomposite for PH sensing, Sensor. Actuator. B Chem. 221 (2015) 993–1002, https://doi.org/10.1016/j.snb.2015.06.095.

[17] S. Islam, N. Bidin, S. Riaz, G. Krishnan, S. Naseem, Sol–gel based fiber optic PH nanosensor: structural and sensing properties, Sensor Actuator Phys. 238 (2016) 8–18, https://doi.org/10.1016/j.sna.2015.12.003.

[18] S.S. Chauhan, R.V. Jasra, A.L. Sharma, Structural, optical, and PH-stimulus response properties of cresol red immobilized nanocomposite silica films derived by a sol–gel process employing different synthetic routes, Ind. Eng. Chem. Res. 53 (49) (2014) 18863–18872, https://doi.org/10.1021/ie500846z.

[19] S. Islam, A. Alshoaibi, O. Saber, H. Bakhtiat, S. Riaz, S. Naseem, Thermally stable mesoporous PH dyes encapsulated titania nanocomposites for opto-chemical sensing, Mater. Res. Bull. 146 (2022) 111605, https://doi.org/10.1016/j.materresbull.2021.111605.

[20] D. Zhao, J. Feng, Q. Huo, N. Melosh, G.H. Fredrickson, B.F. Chmelka, G.D. Stucky, Triblock copolymer syntheses of mesoporous silica with periodic 50 to 300 angstrom pores, Science 279 (5350) (1998) 548–552, https://doi.org/10.1126/science.279.5350.548.

[21] M. Thommes, K. Kaneko, A.V. Neimark, J.P. Olivier, F. Rodriguez-Reinoso, J. Rouquerol, K.S.W. Sing, Physisorption of gases, with special reference to the evaluation of surface area and pore size distribution (IUPAC technical report), Pure Appl. Chem. 87 (9–10) (2015) 1051–1069, https://doi.org/10.1515/pac-2014-1117.

[22] M. Kruk, M.K. Jaroniec, C.H. Ko, R. Ryoo, Characterization of the porous structure of SBA-15, Chem. Mater. 12 (7) (2000) 1961–1968, https://doi.org/10.1021/cm000164e.

[23] J. Torrent, V. Barrón, Diffuse reflectance spectroscopy, ACSESS (2023). https://onlinelibrary.wiley.com/doi/abs/10.2136/sssabookser5.5.c13, 02-28.

[24] A.K. Davey, Z. Li, N. Lefton, B.E. Leonhardt, A. Pourghaderi, S. McElhany, D. Popple, C. Dai, S. Kahn, M.N. Dods, A. Zettl, C. Carraro, R. Maboudian, Enhanced ZIF-8-enabled colorimetric CO2 sensing through dye-precursor synthesis, Sensor. Actuator. B Chem. 374 (2023) 132783, https://doi.org/10.1016/j.snb.2022.132783.

[25] L. Van der Schueren, K. De Clerck, G. Brancatelli, G. Rosace, E. Van Damme, W. De Vos, Novel cellulose and polyamide halochromic textile sensors based on the encapsulation of methyl red into a sol–gel matrix, Sensor. Actuator. B Chem. 162 (1) (2012) 27–34, https://doi.org/10.1016/j.snb.2011.11.077.

[26] É. Bányai, Chapter 3 - acid-base indicators, in: Indicators, E. Bishop (Eds.), International Series of Monographs on Analytical Chemistry, vol. 51, Pergamon, 1972, pp. 65–176, https://doi.org/10.1016/B978-0-08-016617-9.50008-4.

[27] M.M. Ghoneim, Y.M. Issa, M.A. Ashy, Infrared spectra of some derivatives of phenolphthalein & sulphonphthalein, IJC-A 18A (4) (1979) [October 1979].

[28] K. Yamaguchi, Z. Tamura, M. Maeda, Molecular structure of the zwitterionic form of phenolsulfonphthalein, Anal. Sci. 13 (3) (1997) 521–522, https://doi.org/10.2116/analsci.13.521.

[29] C. Rottman, G. Grader, Y. De Hazan, S. Melchior, D. Avnir, Surfactant-induced modification of dopants reactivity in Sol−Gel matrixes, J. Am. Chem. Soc. 121 (37) (1999) 8533–8543, https://doi.org/10.1021/ja991269p.

[30] D. Heger, J. Klánová, P. Klán, Enhanced protonation of cresol red in acidic aqueous solutions caused by freezing, J. Phys. Chem. B 110 (3) (2006) 1277–1287, https://doi.org/10.1021/jp0553683.

[31] I.M. El Nahhal, S.M. Zourab, F.S. Kodeh, F. Babonneau, W. Hegazy, Sol–gel encapsulation of cresol red in presence of surfactants, J. Sol. Gel Sci. Technol. 62 (2) (2012) 117–125, https://doi.org/10.1007/s10971-012-2693-y.

[32] A. Zarinwall, T. Waniek, R. Saadat, U. Braun, H. Sturm, G. Garnweitner, Comprehensive characterization of APTES surface modifications of hydrous boehmite nanoparticles, Langmuir 37 (1) (2021) 171–179.

[33] A. Mahtabani, D. La Zara, R. Anyszka, X. He, M. Paajanen, J.R. van Ommen, W. Dierkes, A. Blume, Gas phase modification of silica nanoparticles in a fluidized bed: tailored deposition of aminopropylsiloxane, Langmuir 37 (15) (2021) 4481–4492, https://doi.org/10.1021/acs.langmuir.0c03647.

[34] B. Qiao, T.-J. Wang, H. Gao, Y. Jin, High density silanization of nano-silica particles using γ-aminopropyltriethoxysilane (APTES), Appl. Surf. Sci. 351 (2015) 646–654, https://doi.org/10.1016/j.apsusc.2015.05.174.

[35] Informatics, N. O. of D. and. Nitrogen dioxide. https://webbook.nist.gov/cgi/cbook.cgi?ID=10102- 44-0..